International Journal of Nanoelectronics and Materials
Volume 13 (Special Issue) Dec 2020 (203-214)

The Design of Monolithic Integration of Photonic Crystal Biosensor to Si-Ge PIN Photodetector on Silicon Photonics Platform for Compact Biosensing System

Mohamad Hazwan Haron[1], Dilla Duryha Berhanuddin[1], Burhanuddin Yeop Majlis[1] and Ahmad Rifqi Md Zain[1*]

[1] *Institute of Microengineering and Nanoelectronics (IMEN), Universiti Kebangsaan Malaysia, 43600 Bangi, Selangor, Malaysia.*

ABSTRACT

The requirements of compact biosensing system features such as portable, wearable and point-of-care applications require compact design solutions. Optical based biosensor is one of the choices because of the high-sensitivity characteristic. In previous researches, one dimensional photonic crystal 1D PhC optical devices have been demonstrated to work as a biosensor by sensing the refractive index (RI) change of its surrounding. However, for the design of a practical biosensing system, the optical signal needs to be converted to the electrical signal by a photodetector for signal processing. Discreet photonics components result in bulky equipments. Compact biosensing system requires compact design solutions. Monolithic integrated design is a good solution to realize this. Here, the optical biosensor component can be monolithically integrated with the photodetector component. There is still no work which shows the integration of the 1D PhC to a photodetector to get an electrical output which is done in this work. In this work, we show the novel design integration of a monolithic integration of 1D PhC biosensor with a Si-Ge PIN photodetector based on silicon photonics platform. The Lumerical software packages are used to simulate the design. Following silicon photonics design methodology, the design and simulations start at the device level for both of 1D PhC biosensor and Si-Ge PIN photodetector components. The extracted data from the device level simulations are used for the circuit level simulations of the integrated 1D PhC-photodetector for electrical output. The simulation results have shown the integrated 1D-PhC design gave good results, which the output of the circuit in electrical domain shows an acceptable power level and the same shift of peak behavior in sensing as from the previous researches in optical domain. The good result suggest that the design data presented in this work can be used further to design a compact optical based biosensing system.

Keywords: Integrated Photonics Design, Optical Biosensor, 1D Photonic Crystal, PIN Si-Ge Photodetector, Silicon Photonics Integrated Circuit.

1. INTRODUCTION

The advances in biomedical fields require advanced biomedical analysis and technologies such as point-of-care diagnosis and wearable healthcare systems [1]. To realize these technologies, compact and portable systems required. Optical type bio-sensing is a good solution because of its good sensitivity characteristic and ability of accurate detection down to a single biological molecule [2][3]. However, conventional discreet photonics results in bulky components and bigger equipments. Photonic integrated circuit (PIC) which offers on-chip photonics integration can be the solution to this problem. Silicon photonics is the most popular platform for the PIC [4], [5]. Silicon photonics uses silicon-on-insulator (SOI) as the main material and offers the

*Corresponding Author: *rifqi@ukm.edu.my*

integration of both passive and active devices on the same chip with the ability to create photonics system-on-chip. It can be the solution in the development of compact and portable biosensing systems.

Photonic crystal (PhC) device can be used for biosensing purpose by sensing the refractive index (RI) change of the target analyte at the sensing region [6][7]. The interaction of the light with the target analyte can either be by the evanescent field that extends to the outside of a straight waveguide [8][9] or by direct propagation through a slotted waveguide. The precise delivery of an analyte to the sensing region can be done by using a microfluidic channel which usually used PDMS material [10]. The measurement of the PhC biosensor can be done by using photonics test equipments like the tunable laser source (TLS) as the light source and optical spectrum analyzer (OSA) as the output monitor. Any changes of RI at the PhC's sensing region will shift the peak signal shown at the OSA. However, for practical biosensing systems, all components must be assembled together. A simple optical biosensing system architecture is shown in figure 1[11]. It is the combination of photonics and electronics parts to make a complete system. The photonics components consist of a light source, an optical biosensor and a photodetector. The electronics components consist of the transimpedance amplifier (TIA), analog to digital converter (ADC), and the digital signal processing (DSP) unit.

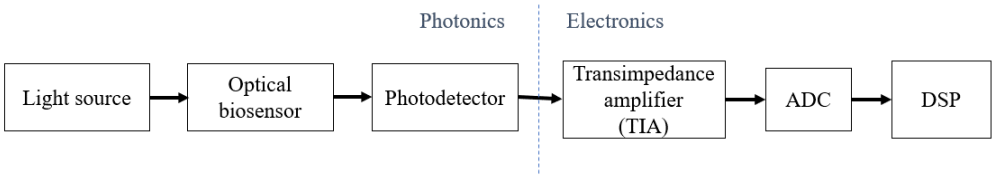

Figure 1. A common architecture of an optical biosensing system.

However, for the compact system requirements, all components must be miniaturized and very compact. At the devices level, because device packaging increases the allocated size of a system, then reducing the packaging number can be the solution. This can be done by the integrated design. Silicon photonics offers the capability to do this. For this to happens, a proper silicon photonics design flow which is almost similar with the CMOS design flow has been developed [12]. An example of high-density silicon photonics is the wavelength division multiplexing (WDM) for receiver applications. The multi-channels WDM can be integrated directly to the photodetector on the same chip [13]. This work focuses on one-dimensional photonic crystal (1D PhC) device as the biosensor. 1D PhC structure with a cavity can a give high quality factor (Q-factor) output signal [14], [15]. For a biosensing system design, the optical signal which comes from the optical biosensor must be converted into an electrical signal by using a photodetector for further signal amplification and processing.

To make a compact biosensing system, on-chip integration of optical biosensor with the photodetector can be the solution. Several works have shown the integration of optical sensor with a photodetector to realize this [16], [17]. However, there is still no work which shows the integrated design of PhC biosensor device with the photodetector for direct optical detection to electrical signal conversion which will be done in this work. In this work, we design the integration of the one-dimensional photonic crystal (1D PhC) as the biosensor with a PIN silicon-germanium (Si-Ge) photodetector for the use of very compact biosensing systems, targeting either for portable, handheld or wearable applications. The Si-Ge materials are good choice for the integrated silicon photonics design because the germanium can compensate the lack of absorption of Si in the range of around 1550 nm wavelength and has been demonstrated in previous researches [18][19]. The 1550 nm at the communication band (c-band) is a choice here because of the existing measurement instruments for this band and it also response well to the biomolecule detection which makes it good for biosensing.

One of the most important characteristics to design a photodetector is to have enough responsivity. The responsivity is given by $R = I / P$ (A/W) where P is the incident power and I is the electrical current. It is the ration of generated photocurrent to the incident power. In term of the quantum efficiency, the responsivity is given by,

$$R = \eta \frac{q\lambda}{hc} \tag{1}$$

Where η is the quantum efficiency, q is the charge of an electron, λ is the wavelength of light, h is the Planck's constant and c is the speed of light. The relationship of the absorbed power in a photodetector is given as,

$$P_{\text{abs}} = P_{in} - P_{tr=} P_{in}(1 - e^{-\alpha L}) \tag{2}$$

Where P_{in} is the power of incident light, P_{tr} is the transmitted power, α is the absorption coefficient and L is the length of the photodetector. The equation shows that the absorption which leads to the responsivity increases logarithmically with the photodetector's length. Hence, the photodetector's length can be increased to find the best responsivity can be achieved.

The design of a photodetector which is compatible with the silicon platform is important to solve the integration issue. Table 1 compares several photodetector structures which are compatible with silicon photonics platform. Comparing the figure-of-merits (FOM) from these works, the results of photodetector design should be obtained in our work is to be more than 1 A/W for the responsivity while having reasonable dark current. The final important parameter to be observed is the power level of the sensing peak.

Table 1 The comparison of data of Si based photodetector from previous researches

Material	Photodetector Length (μm)	Bias voltage (V)	Dark current (nA)	Responsivity (A/W)	Ref
Si-Ge	10	-1	11	1.05	[20]
Si-Ge	50	-2	169	1.16	[21]
Si-Ge	10	-1	4000	0.8	[22]
Si-InGaAs	40	0 to -10	0.01	1.1	[23]

By monolithically integrating the PhC biosensor with the photodetector, the shift of peak in electrical signal when there is a change in the surrounding RI has been obtained with a single chip design. The results obtained from this work show that the design is successful and suggest that it can be used to solve the compact biosensing system design. This work has also expanded the photonic crystal-based works to the more practical integrated design for real applications and advanced technology in the biomedical fields.

2. METHODOLOGY

The general design methodology follows the common silicon photonics design flow which starts from devices design and simulation, followed by parameter or data upload to the PIC level simulation and constructing the GDS layout for fabrication. The full silicon photonics design flow is shown in figure 2. This work goes from component modeling and simulation, then PIC level simulation, and finally physical layout.

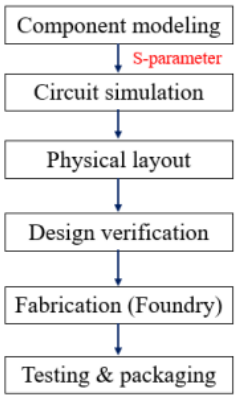

Figure 2. Silicon photonic system design flow [24].

The design and simulations are done by using the Lumerical software package. The Lumerical MODE is used to calculate the effective index of a 500 x 220 nm waveguide. The calculated effective index (N_{eff}) will be used in Lumerical FDTD calculation. The S-parameter of the 1D PhC device will be extracted for the PIC level simulation. Then, the design and simulation of the PIN Si-Ge photodetector will be done by using Lumerical Device and FDTD software. The final calculated dark current and responsivity of the designed photodetector will be used for the PIC level simulation in Lumerical Interconnect. The full design flow used in this work is shown in figure 3.

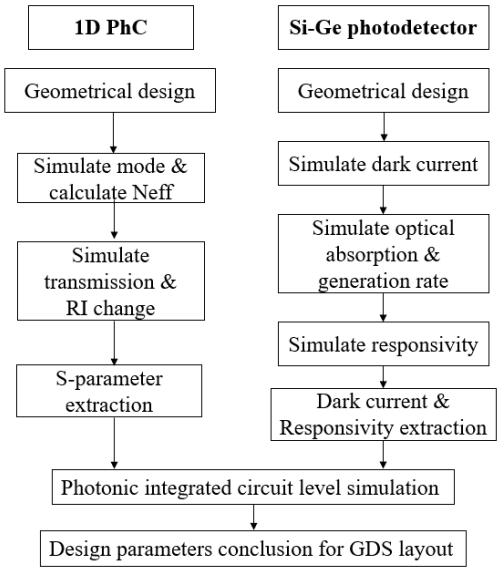

Figure 3. The design and simulations flow of the integrated PhC biosensor with PIN Si-Ge photodetector.

2.1 1D PhC Biosensor Design

To simulate the 1D PhC device as the biosensor using the 2.5 FDTD method, first the N_{eff} of the waveguide that will be used for the device must be calculated. The waveguide used is 500 x 220 nm SOI, which the Si thickness is 220 nm. The calculation of the Neff is done by using Eigenmode solver in Lumerical MODE. The calculated Neff is used in 2D FDTD solver, which makes it 2.5D FDTD simulation [25], [26]. The 1D PhC device's parameters are shown in figure 4, which *a* is the lattice constant, *c* is the cavity length, and *r* is the hole's radius. For the 1D PhC design parameters used for the simulation, *a* is 400 nm, *c* is 480 nm, *r* is 50 nm and the number of holes, N is 40. To

show its sensing response to the RI change, the RI of the surrounding background is changed in the 2.5D FDTD simulation. Finally, the S-parameter of the designed 1D PhC biosensor is extracted and will be used in the PIC level simulation.

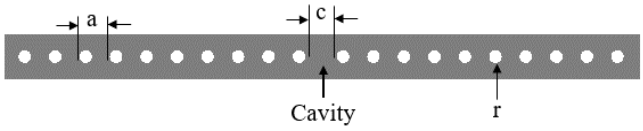

Figure 4. Top view of 1D PhC structure and its parameters.

2.2 Si-Ge PIN Photodetector Design

The cross-section of the designed photodetector is shown in figure 5. The designed photodetector is PIN Si-Ge photodetector. The contacts' material is aluminium (Al). the anodes are on the sides of the Si rib waveguide and the cathode is on top of the Ge n+ layer. the width of the Ge layer is 4 µm, the height is 1 µm and the length is varied from 10 to 100 µm for the simulation to find the suitable responsivity. The doping concentration is $10^{18}cm^{-3}$ for p, $10^{19}cm^{-3}$ for n+ and 10^{20} for p++.

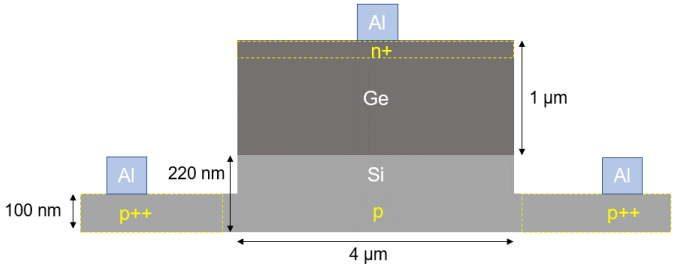

Figure 5. The cross-sectional view of the designed PIN Si-Ge photodetector and its parameters.

The simulation of the dark current is done by using CHARGE solver in Lumerical DEVICE. To simulate the dark current, the anode is swept from 0 to -2V to give a reverse bias. The cathode is set to constant 0V during the swept. The voltage difference between the anode and cathode will create an electric field which will sweep the photoelectron out of the intrinsic region. The simulation with the swept voltage was repeated for photodetector lengths from 10 to 100 µm.

2.3 PIC Schematic Design

The PIC schematic is the combination of compact models of each component. To simulate the monolithic integration of 1D PhC to Si-Ge PIN photodetector, a schematic was drawn in lumerical Interconnect as shown in figure 6 which consists of the compact models of 1D PhC and PIN Si-Ge Photodetector. To test this integrated schematic behavior, the continuous wave laser was used as the light source and the electrical power meter was placed after the photodetector component to monitor the peak's power in electrical signal. To complete the setup of the schematic, the extracted S-parameter from the Lumerical FDTD simulation was uploaded into the 1DPhC component, then the dark current and responsivity values were set into the PIN photodetector component. The laser source was set to 0 dBM as the reference power and was swept through the wavelength.

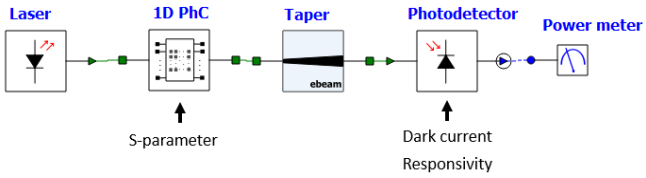

Figure 6. The PIC schematic to simulate the monolithic integration of 1D PhC biosensor to Si-Ge PIN photodetector with the uploaded data into each compact model.

3. RESULTS AND DISCUSSION

3.1 Results of 1D PhC

The simulated mode profile of the 500 x 220 nm SOI is shown in figure 7 which shows acceptable light confinement and the evanescent field which extends to the outside of the waveguide is utilized for different RI sensing at its srrounding. The calculated N_{eff} of the fundamental TE mode is 2.4445.

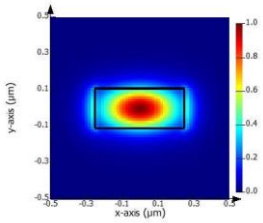

Figure 7. Mode profile of a 500 x 220 nm waveguide.

The transmission result of the 2.5D FDTD simulation of the 1D PhC is shown in figure 8(a), where the peak is located at 1550 nm wavelength with a transmission of 0.77. The calculated Q-factor is 9579. The transmission loss of 0.33 is acceptable to obtain the high Q-factor value which would be more accurate in sensing because of the sharpness of the peak. Figure 8(b) shows the simulation of the RI change around the device, which results in the shift of the peak. The S-parameter of the 1D PhC device based on the result in figure 8(a) is extracted for the PIC level simulation in Lumerical Interconnect.

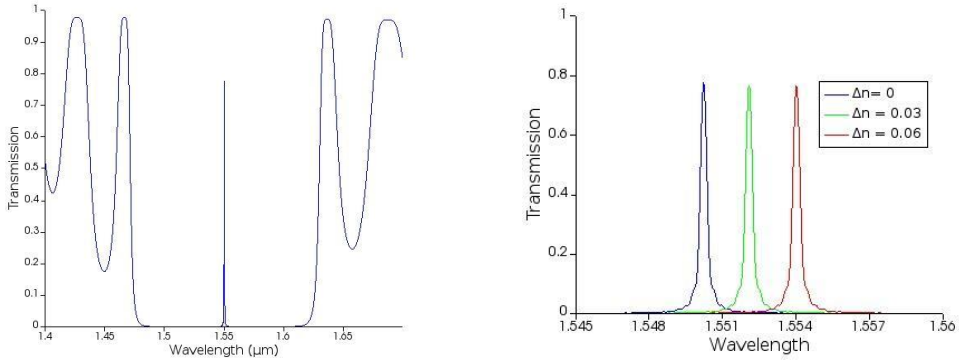

(a) (b)

Figure 8. (a) The transmission of the designed 1D PhC for biosensing, and (b) The shift of the peak when there is a RI change at the surrounding.

3.2 Results of Photodetector

The transition of light from the Si waveguide into the Ge layer is shown in figure 9. The light at around 1550 nm will be absorb more inside the Ge layer compared to Si layer because of its absorption charactersitic.

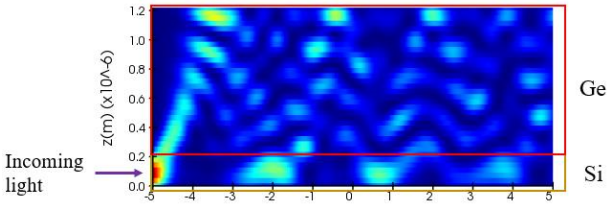

Figure 9. The electric field profile showing the the transition of light from the Si waveguide into the Ge layer.

The results of the dark current simulation are shown in figure 10, where figure 10(a) shows the change of dark current in term of increasing reverse bias voltage at anode, and figure 10(b) shows the change of dark current in term of the photodetector's length at -2V bias. Figure 10(a) shows as the magnitude of the bias voltage increases, the value of the dark current increases from 0. A longer photodetector's length results in higher dark current at the same bias voltage. The data of the calculated dark current at -2V is inserted into the PIC level simulation in Lumerical Interconnect.

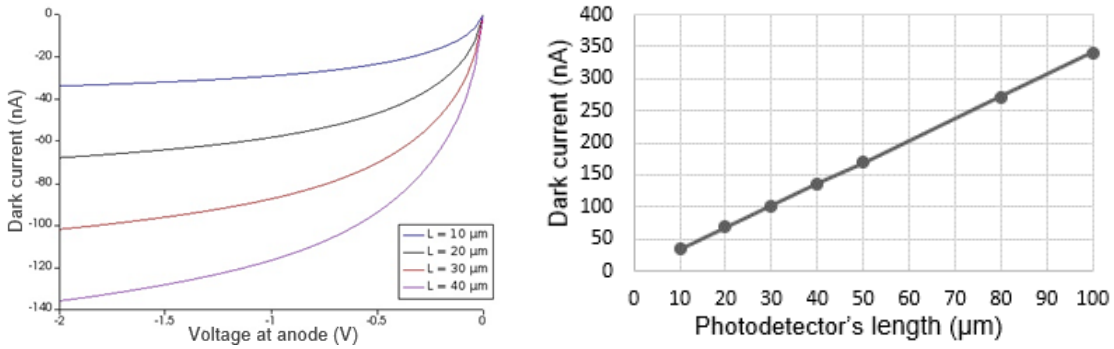

(a) (b)

Figure 10. (a) The generated current with the variations of voltage and photodetector's length. (b) Dark current vs photodetector's length.

The next step is the optical absorption simulation which will be done with 3D FDTD solver in Lumerical FDTD for the same photodetector's design. The results of the simulations are shown in figure 11 and figure 12. Figure 11 shows the generation rate profile across the middle of the photodetector from top view. As the photodetector's length increases, the generation rate at the end of the photodetector's becomes weaker.

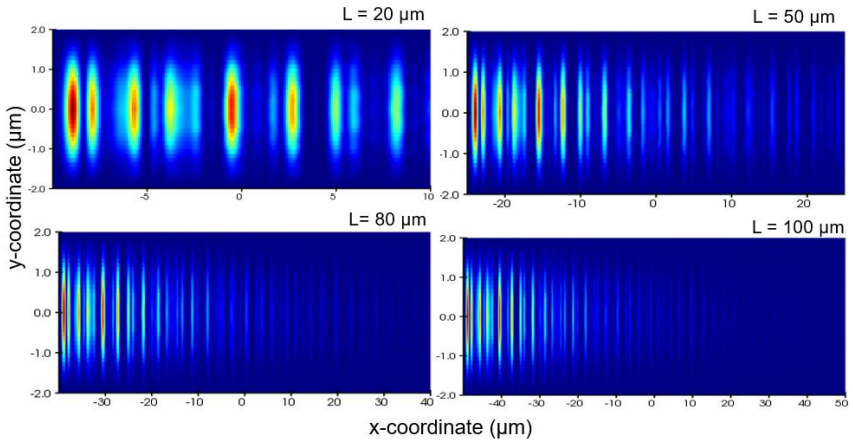

Figure 11. The generation rate profile over the photodetector's length.

Figure 12(a) shows the plot of calculated total power absorbed (P_t) with increasing photodetector's length, where P_t of 1 equal 100 % absorbed power from the incoming light. The plot shows that at L = 50 µm, P_t starts to saturate as the total absorbed power comes close to 1. At L = 100 µm, P_t is completely saturated at 0.9408. figure 12(b) shows the plot of the calculated responsivity with increasing photodetector's length. The responsivity starts to saturate when L = 50µm. At L = 100 µm, the responsivity is already saturated at the value of 1.204 A/W. The saturation is because the total absorbed power is already saturated as shown in figure 12(a). This means a photodetector's length longer than 100 µm is not needed for the designed photodetector.

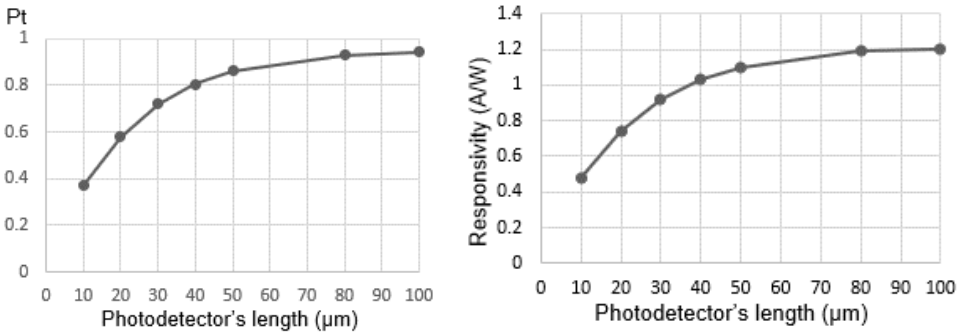

(a) (b)

Figure 12. (a) Total power absorbed vs photodetector's length. (b) Responsivity vs photodetector's length.

3.3 Results of PIC

The simulation of the PIC schematic shown in figure 6 was done in Lumerical Interconnect and the calculated peak's power in electrical signal for every L is shown in figure 13(a). The detecteed peak's power increases from -84.19 dBM to -75.96 dBM as L increases untul it saturated which is related to the saturation of the responsivity and P_t in figure 12(a) and 12(b). the shift of peak in electrical signal when there is a change in the surrounding RI is shown in figure 13(b). These results show that the design of the integrated 1D PhC biosensor to the PIN Si-Ge photodetector is seccessful. However, to be practical in further signal processing part, a transimpedance amplifier (TIA) is needed to amplify the signal to an acceptable level to the DSP unit.

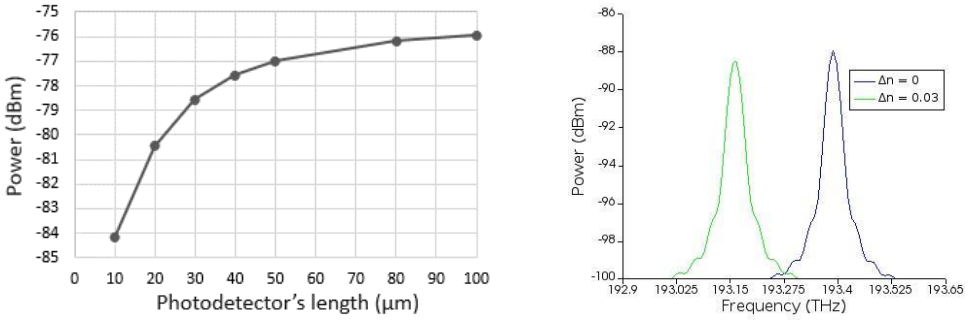

Figure 13. The shift of peak with RI change in electrical signal.

The data obtained from this work are listed in table 2. The data shows that as L increases, the dark current will keep increasing linearly. As P_t increases and saturated to almost 1, the responsivity will increase until it is saturated at around 1.2 A/W. The power level of the detection peak follows the same pattern as P_t and responsivity. The dark current is considered as noise and usually the minimization of it is required. The results show that there is a tradeoff between the dark current and responsivity. Because the dark current keeps increasing linearly as L increases while the responsivity starts to saturate at around L = 40 μm, one of the best choice for the signal to noise ratio (SNR) is to choose L = 50 μm, thus we get the responsivity of 1.1879 A/W and the dark curret of 169.95 nA.

Table 2 The simulation data of the designed monolithic integration of 1D PhC biosensor to Si-Ge PIN photodetector

Photodetector's length	Dark current (nA)	P_t	Responsivity	EPM (dBm)
10	33.90	0.3711	0.474	-84.19
20	67.98	0.5781	0.74	-80.46
30	101.93	0.7206	0.9221	-78.57
40	135.91	0.8054	1.0316	-77.58
50	169.95	0.8599	1.1014	-76.98
80	271.82	0.9277	1.1879	-76.18
100	339.90	0.9408	1.204	-75.96

The results show that the behavior at the PIC level of the 1D PhC biosensor with the Si-Ge PIN photodetector is as needed, hence this work is successful. However, after the final GDS layout design for fabrication, extra components need to be considered for the simulation such as the straight waveguide length and the light coupler which would add more losses of light.

The illustration of the GDS layout design (not to scale) without the doping layers is shown in figure 13. The layout design follows the generic silicon photonics technology (GSiP) design rules mentioned in reference [24]. The layout shows that the Si layer extends from the 1D PhC component until the base of the Si-Ge photodetector. The M2 wireguides connect the photodetector's contacts to the electrical pads and bias circuit.

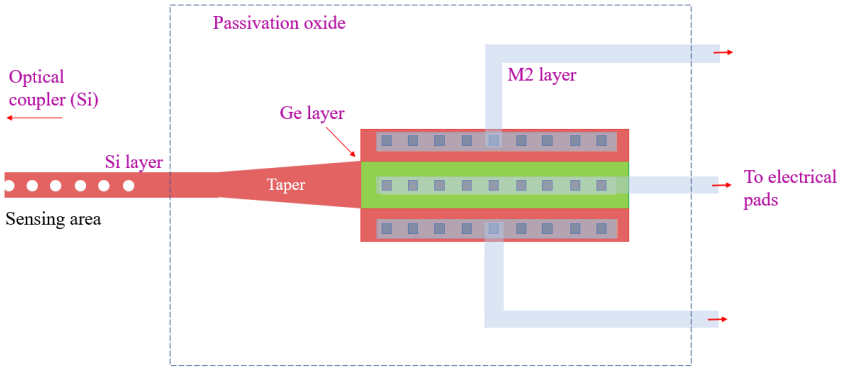

Figure 14. The illustration of the GDS layout design (not to scale) without the doping layers, following the generic silicon photonics (GSiP) technology design rules and layers arrangement.

4. CONCLUSION

We have designed and simulate a monolithic integration of 1D PhC biosensor to Si-Ge PIN photodetector based on silicon photonics platform which uses SOI as the main material. The design uses silicon photonics design methodology which starts from the device level and and up to PIC level design and simulation. The output of the 1D PhC with a cavity is a single peak signal at 1550 nm wavelength with the calculated Q-factor of 9579. The simulation of the RI change which indicates the change in an analyte's concentration at the sensing region of the 1D PhC biosensor has shown the shift of the peak which can be used for signal processing. The S-parameter from the 1D PhC simulation has been extracted for circuit level simulation. The simulation of the photodetector has been done to determine the effect of the photodetector's length to the dark current and responsivity. These two calculated values are used in the circuit level simulation. The results of total power absorbed and the generation rate profile for each photodetector's length have suggested that there is no need to use the designed photodetector longer than 100 µm. The simulation of the integration of 1D PhC and Si-Ge PIN photodetector has been done in Lumerical Interconnect for each of the photodetector's length data. The ouput power of the circuit is from -84.19 to -75.96 dBm, which suggest the use of TIA for further signal processing part. There is a tradeoff between the dark current and the responsivity when increasing *L*. The design data presented in this work was successfully verified by the simulation tools and proved it can be useful for the design of compact biosensing system.

ACKNOWLEDGEMENTS

This research is supported by FRGS/1/2015/TK04/UKM/02/4 grant funded by the Ministry of Higher Education (MOHE) Malaysia.

REFERENCES

[1] S. Panesar, X. Weng, & S. Neethirajan, "Towards Point-of-care Diagnostics of Breast Cancer: Development of an Optical Biosensor Using Quantum Dots," **2**, 3 (2017) pp. 2–5.
[2] S. M. Borisov & O. S. Wolfbeis, "Optical Biosensors," chem Rev. **108** (2008) 423–461.
[3] X. Fan, I. M. White, S. I. Shopova, H. Zhu, J. D. Suter, Y. Sun, "Sensitive optical biosensors for unlabeled targets: A review," Anal. Chim. Acta **620**, 1–2 (2008) 8–26.

[4] J. E. Bowers *et al.,* "Recent Advances in Silicon Photonic Integrated Circuits," in Next-Generation Optical Communication: Components, Sub-Systems, and Systems V **9774** (2016) 1–18.
[5] P. P. Absil, P. Verheyen, P. De Heyn, M. Pantouvaki, G. Lepage, "Silicon photonics integrated circuits: a manufacturing platform for high density, low power optical I / O ' s," **23**, 7 (2015) 9369–9378.
[6] F. Liang, N. Clarke, P. Patel, M. Loncar, & Q. Quan, "Scalable photonic crystal chips for high sensitivity protein detection," **21**, 26 (2013) 6071–6077.
[7] N. Skivesen, A. Têtu, M. Kristensen, & D.-K. Lyngby, "Photonic-crystal waveguide biosensor," **15**, 6 (2007) 3169–3176.
[8] F. Prieto *et al.,* "An integrated optical interferometric nanodevice based on silicon technology for biosensor applications," Nanotechnology **14**, 8 (2003) 907–912.
[9] S. A. T. A. F. Ard *et al.,* "Optimized sensitivity of silicon-on-insulator (SOI) strip waveguide resonator sensor," **8**, 2 (2017) 654–661.
[10] P. Abgrall & A.-M. Gué, "Lab-on-chip technologies: making a microfluidic network and coupling it into a complete microsystem -a review," J. Micromech. Microeng. **17** (2007) R15–R49.
[11] J. P. Bentley, Principles of Measurement Systems, Fourth. Malaysia: Pearson Education Limited, (2005).
[12] L. Chrostowski *et al.,* "Design methodologies for silicon photonic integrated circuits," in Smart Photonic and Optoelectronic Integrated Circuits XVI **8989** (2014) 1–15.
[13] "25 × 50 Gbps wavelength division multiplexing silicon photonics receiver chip based on a silicon nanowire-arrayed waveguide grating.pdf."
[14] A. R. Md Zain, M. Gnan, H. M. H. Chong, M. Sorel, R. M. De La Rue, "Tapered photonic crystal microcavities embedded in photonic wire waveguides with large resonance quality-factor and high transmission," IEEE Photonics Technol. Lett. **20**, 1 (2008) 6–8.
[15] A. R. Zain *et al.,* "Ultra high quality factor one dimensional photonic crystal / photonic wire micro-cavities in silicon-on-insulator (SOI)," **16**, 16 (2008) 12084–12089.
[16] D. Ahn *et al.,* "High performance, waveguide integrated Ge photodetectors," **15**, 7 (2007) 3916–3921.
[17] J. Song *et al.,* "Silicon-based optoelectronic integrated circuit for label-free bio / chemical sensor," **21**, 15 (2013) 2528–2533.
[18] Y. Zhang *et al.,* "A high-responsivity photodetector absent metal- germanium direct contact," **22**, 9 (2014) 11367–11375.
[19] J. K. Doylend, P. E. Jessop, A. P. Knights, "Silicon photonic resonator-enhanced defect-mediated photodiode for sub-bandgap detection," **18**, 14 (2010) 14671–14678.
[20] S. Liao *et al.,* "36 GHz submicron silicon waveguide germanium photodetector," **19**, 11 (2011) 10967–10972.
[21] T. Yin et al., "31GHz Ge n-i-p waveguide photodetectors on Silicon-on-Insulator substrate Abstract," **15**, 21 (2007) 13965–13971.
[22] L. Vivien *et al.,* "Zero-bias 40Gbit / s germanium waveguide photodetector on silicon," **20**, 2 (2012) 5905–5907.
[23] Z. Sheng, L. Liu, J. Brouckaert, S. He, & D. Van Thourhout, "InGaAs PIN photodetectors integrated on silicon-on-insulator waveguides," **18**, 2 (2010) 411–414.
[24] L. Chrostowski & M. Hochberg, Silicon Photonics Design: From Devices to Systems. Glasgow: Cambridge University Press, (2015).
[25] M. Hammer, O. V Ivanova, "Effective index approximations of photonic crystal slabs: a 2-to-1-D assessment," (2009) 267–283.
[26] H. G. Danielmeyer, W. Streifer, D. R. Scifres, G. Fonstad, T. Oaks, "The Effective Index Method and Its Application to Semiconductor Lasers," 7 (1982) 1083–1089.